Achieving Geodetic Motion for LISA Test Masses: Ground Testing Results

L. Carbone,[1] A. Cavalleri,[2] R. Dolesi,[1] C. D. Hoyle,[1] M. Hueller,[1] S. Vitale,[1] and W. J. Weber[1]

[1]*Dipartimento di Fisica, Università di Trento, and I.N.F.N., Gruppo di Trento, 38050 Povo (TN), Italy*

[2]*Centro Fisica degli Stati Aggregati, 38050 Povo (TN), Italy*

(Received 1 July 2003; published 8 October 2003; publisher error corrected 10 October 2003)

The low-frequency resolution of space-based gravitational wave observatories such as LISA (Laser Interferometry Space Antenna) hinges on the orbital purity of a free-falling reference test mass inside a satellite shield. We present here a torsion pendulum study of the forces that will disturb an orbiting test mass inside a LISA capacitive position sensor. The pendulum, with a measured torque noise floor below 10 fN m/$\sqrt{\text{Hz}}$ from 0.6 to 10 mHz, has allowed placement of an upper limit on sensor force noise contributions, measurement of the sensor electrostatic stiffness at the 5% level, and detection and compensation of stray dc electrostatic biases at the millivolt level.

DOI: 10.1103/PhysRevLett.91.151101 PACS numbers: 04.80.Nn, 07.87.+v, 95.55.Ym

Among the most challenging technologies needed for the LISA gravitational wave mission is that of placing test masses in pure free fall. Accelerations due to stray forces change the distance between orbiting test masses, directly contaminating an interferometric measurement of gravitational wave strain. The LISA sensitivity goal requires acceleration noise a_n with spectral density below 3×10^{-15} m/s^2/$\sqrt{\text{Hz}}$ at frequencies down to 0.1 mHz or force noise of order fN/$\sqrt{\text{Hz}}$ for a $\sim$1 kg test mass [1].

Environmental force noise can be screened by a satellite shield employing precision thrusters and a relative position sensor to remain centered about the free-falling test mass. The satellite, however, creates disturbances, particularly due to the close proximity of the position sensor. While noise analyses have shown proposed electrostatic sensor designs [2,3], with 2–4 mm test mass–sensor separations, to be compatible with the LISA goals, the low frequencies and extreme force isolation goals require force disturbance measurements to provide confidence in the LISA sensitivity predictions.

An ideal test of stray forces for LISA compares the differential noise in the orbits of two nearby free-falling test masses. This test will be performed, with a target acceleration noise limit of 30 fm/s^2/$\sqrt{\text{Hz}}$ at 1 mHz, by the LISA Test-flight Package (LTP) [4] and ST-7 [5]. In preparing for such flight tests, we study the forces acting on a test mass that is nearly "free" in a single rotational degree of freedom, suspended by a thin torsion fiber inside a capacitive position sensor. The thermal torque noise limit, approached in similar apparatuses [6], is several fN m/$\sqrt{\text{Hz}}$ at 1 mHz for the torsion pendulum used here [7]. Dividing by half the 40 mm test mass width, this converts to a force noise of order 100 fN/$\sqrt{\text{Hz}}$, within a factor 100 (10) of the LISA (LTP/ST-7) force noise target.

The translational acceleration noise relevant to LISA can be divided into contributions from random forces f_{str} acting on the test mass (mass m) and from coupling to the relative motion of the satellite (mass M) via any dc force gradient (or "stiffness") k_p. The spacecraft motion noise arises in the position sensing noise x_n and in the imperfect compensation of the external forces F_{str} acting on the satellite by the finite gain control loop (gain ω_{DF}^2). The residual acceleration noise a_n is

$$a_n = \frac{f_{\text{str}}}{m} + \frac{k_p}{m}\left(x_n + \frac{F_{\text{str}}}{M\omega_{\text{DF}}^2}\right). \tag{1}$$

To characterize a_n, we use the torques, measured from the pendulum twist ϕ, acting on a LISA-like test mass inside a realistic capacitive position sensor designed for LISA's sensing noise (spectral density $S_{x_n}^{1/2} \sim$ nm/$\sqrt{\text{Hz}}$) and electrostatic force gradient ($k_p \sim 100$ nN/m) requirements. The measured pendulum angular noise in the LISA measurement band establishes an upper limit on the contribution of noisy surface forces to f_{str}. Measurement of the rotational stiffness due to the ac sensing voltage characterizes a key part of the translational stiffness k_p. Finally, measurement and compensation of the sensor rotational electrostatic bias imbalance quantify and demonstrate neutralization of a potentially important contribution of stray dc electric fields to f_{str}.

The capacitive position sensor tested here (sketched in Fig. 1 and discussed in Refs. [8,9]) is a variation of that projected for LTP [2,10]. With the 40 mm test mass centered, the gap d between all electrodes and the mass is 2 mm. The electrodes are gold coated Mo and are separated from the electrically grounded Mo housing by ceramic spacers. Differential gap sensing measurements from six sensing electrode pairs are combined to yield the three translational and three rotational test mass displacements. The sensor noise floor is dominated by transformer thermal noise, with $S_{x_n}^{1/2} \approx 0.3$ nm/$\sqrt{\text{Hz}}$ and $S_{\phi_n}^{1/2} \approx$ 40 nrad/$\sqrt{\text{Hz}}$. Integrated actuation circuitry can apply voltages to the sensing electrodes, used here for occasional pendulum control in ϕ and for electrostatic characterization of the sensor. All electrode surfaces have a dc path to a single circuit ground.

The main pendulum component is the test mass itself, a hollow gold coated Ti cube nominally 40 mm on a side, with 2 mm walls. The test mass hangs inside the sensor, connected to the torsion fiber by an Al shaft passing

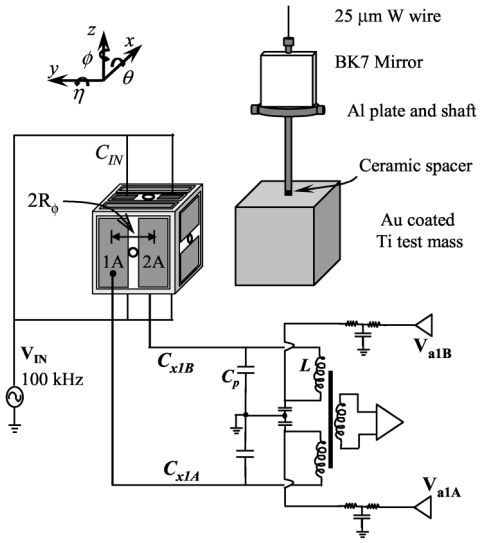

FIG. 1. Sensor electrode configuration and circuitry, with pendulum shown at right. A 100 kHz excitation voltage is applied capacitively through four injection electrodes located on the sensor z faces. Each of six sensing electrode pairs is read out by a resonant inductive bridge circuit ([8], shown here for pair 1). The sum of the signals from pairs 1 and 2 gives the translation in x, and the difference, combined with the on-center electrode separation $2R_\phi = 20.5$ mm, gives the rotation ϕ about the torsion fiber axis. Actuation voltages (V_{a1A} and V_{a1B} for pair 1) can be applied to each electrode through the bridge circuitry. The nominal test mass capacitances to each injection electrode, each $x\phi$ sensing electrode, and to the entire sensor are, respectively, $C_{IN} \approx 0.6$ pF, $C_x \approx 2$ pF, and $C_T \approx 40$ pF, and the excitation $V_{IN} = 6V_{\rm rms}$ ac biases the test mass to $\alpha V_{IN} \approx 0.4V_{\rm rms}$, where $\alpha \equiv 4C_{IN}/C_T$.

through a hole on the top z face of the sensor. The shaft supports an Al stopper plate, which limits the pendulum torsional range, and a silvered glass mirror, which allows an independent autocollimator readout of the pendulum torsional (ϕ) and swing (η) angles. The shaft assembly is grounded through the torsion fiber and isolated from the test mass by a ceramic spacer. The total pendulum mass is 101.4 g (the test mass weighs 80.6 g) and has a calculated moment of inertia $I = 338 \pm 5\ \mathrm{g\,cm^2}$.

The torsion fiber is a nominally 25 μm W wire of length 1 m. It hangs from an upper pendulum stage with an eddy current magnetic damper, which damps the pendulum swing mode with a 200 s decay time. The pendulum and sensor are mounted on independent micropositioners, allowing a 6 degree of freedom adjustment of the relative position of test mass inside the electrode housing. The apparatus vacuum chamber is evacuated below 10^{-5} mbar and sits in a thermally controlled room with 50 mK long term stability.

With the sensor excitation on, the free torsional oscillation period T_0 is 515.1 s, with a quality factor $Q \approx 1700$. The period falls to 510.3 s with the sensor bias off (the period change is due to a negative torsional sensor stiffness, to be discussed shortly). These pendulum dynamics, combined with the calculated moment of inertia, allow conversion of measured angular deflections in ϕ into torques, using the transfer function

$$N(\omega) = \phi(\omega) \times I\omega_0^2\left[1 - \left(\frac{\omega}{\omega_0}\right)^2 + \frac{i}{Q}\right], \qquad (2)$$

where $\omega_0 = 2\pi/T_0$ and we assume a frequency independent pendulum loss angle $1/Q$.

Figure 2 shows typical torque noise data, calculated from the pendulum angular noise using Eq. (2). Also shown is the instrument limit given by the quadrature sum of the pendulum thermal noise, $S_{N,\rm th}^{1/2} = \sqrt{4k_BT(I\omega_0^2/\omega Q)}$, and the sensor readout noise, $S_{\phi_n}^{1/2}$, converted into torque noise, which dominates above 5 mHz. Near 1 mHz, the raw torque noise is roughly 10 times the thermal limit. We found the main excess noise source to be a coupling to translational motion between the sensor and pendulum, due to laboratory tilt noise. This coupling, with magnitude of order 10^{-7} Nm/m, is considerably stronger than reported torsion fiber "tilt-twist" couplings [6] and is likely related to an electrostatic interaction involving the dielectric mirror edges. To better characterize the sensor contribution to $f_{\rm str}$, in the absence of this coupling to laboratory motion, we calculate the instantaneous coupling torque and subtract the resultant twist from the ϕ time series. The tilt, measured in the x and y sensor readouts, is converted to torque through the measured tilt-twist coupling coefficients and then to angular twist through the pendulum transfer function [Eq. (2)]. The remaining torque noise is roughly twice the pendulum thermal noise at millihertz frequencies and below 10 $\mathrm{fN\,m/\sqrt{Hz}}$ from 0.6 to 10 mHz. The excess low-frequency noise is highly correlated with the temperature fluctuations, but, to avoid subtracting a possible sensor-related temperature effect, no further correction has been made.

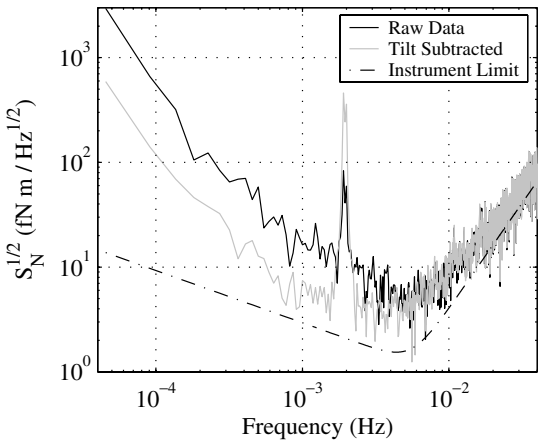

FIG. 2. Plot showing the raw (dark line) and tilt subtracted (light line) pendulum torque noise, with the instrument limit (dashed line). Spectra for this 19 h measurement are calculated with a 22 000 s Hanning window, which leaves an artificial peak near the 2 mHz pendulum resonance.

The low noise pendulum allows precise measurement of coherently modulated torque disturbances; we present here two such measurements. The first concerns the electrostatic stiffness [8–10] associated with the 100 kHz sensor excitation voltage. In the approximation that all electrode surfaces i are grounded, directly or by the readout circuitry, the test mass feels a negative electrostatic spring proportional to the square of the bias amplitude, in rotation as well as translation. Considering only the dc average $\langle V_{IN}^2 \rangle$, ignoring the torque at 2×100 kHz, the stiffness torque is given by

$$N = \frac{\alpha^2 \langle V_{IN}^2 \rangle}{2} (\phi - \phi_0) \sum_i \left(\frac{\partial^2 C_i}{\partial \phi^2} \right) \equiv -\Gamma_s (\phi - \phi_0). \quad (3)$$

Here ϕ_0 is the (unstable) electrostatic equilibrium angle where this torque vanishes.

To measure the sensing stiffness Γ_s, we modulate the effect by switching the $6V_{\rm rms}$ injection voltage on and off at frequency $f_m = 5$ mHz. The resultant pendulum deflection, measured by the autocollimator, is proportional to Γ_s, and the amplitudes at odd multiples of f_m reflect the $1/f$ dependence of the square wave torque's Fourier coefficients. The measurement is made over a range of test mass angles ϕ by rotating the pendulum suspension point. Linear fitting of torque amplitude versus ϕ for each odd harmonic of f_m gives estimates of Γ_s and ϕ_0 (the latter measured relative to the sensor zero).

Figure 3 shows modulated stiffness torques for the first three odd harmonics of f_m. The resulting estimates for Γ_s and ϕ_0, shown with their statistical uncertainties in Table I, are in agreement for the three harmonics. Though the statistical resolution for Γ_s (for $1f_m$) in a given measurement is below 1%, repeated measurements have yielded a scatter of $\pm 5\%$, which is currently being investigated. The measurement has also been performed at a fixed angle for a range of V_{IN}, verifying the expected $\Gamma_s \propto \langle V_{IN}^2 \rangle$ dependence. The range of Γ_s measured with the modulation technique is consistent with the observed period change for sensor bias on and off, which yield $\Gamma_s = -96 \pm 3$ fN m/mrad. A prediction for Γ_s obtained using a finite element capacitance calculation [11] gives -96 ± 5 fN m/mrad, with the uncertainty dominated by machining tolerances. The measured several milliradian offsets between the torque and sensor zeros, which would coincide in a geometrically perfect sensor, are also consistent with the machining tolerances.

Another potentially important noise source for LISA is stray dc electrostatic fields, associated with patch or surface contamination effects. A charged test mass feels force (torque) proportional to the net linear (rotational) imbalances in the electrostatic potential on the surrounding sensor surfaces. For the cosmic ray charging expected for LISA [12], net dc potential imbalances of order 10 mV can produce significant low-frequency acceleration noise [10,13]. To measure dc imbalances, we simulate a charge modulation by biasing the mass with a voltage

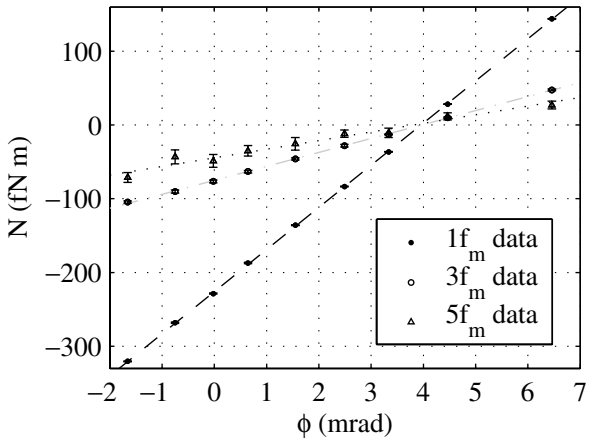

FIG. 3. Plot showing the $1f_m$, $3f_m$, and $5f_m$ (5, 15, and 25 mHz) torque components in the stiffness measurement. The roughly 5:3:1 ratio of the slopes corresponds to the $1/f$ square wave spectral content. The sub–fN m resolution for the $1f_m$ data is smaller than the point markers.

$V_\Delta \sin 2\pi f_m t$ applied to the injection electrodes and measure the resulting pendulum torque [14].

Assigning a mean stray dc voltage δV_i to each conductor, the $1f_m$ torque produced in this measurement is

$$N_{1f_m} = -\alpha V_\Delta \sin 2\pi f_m t \times \sum_i \left(\frac{\partial C_i}{\partial \phi} \right) \delta V_i. \quad (4)$$

In principle, to reflect the electrostatic potential nonuniformity, the sum over electrodes i should be an integral over all surface domains with different potentials. In the naive but useful model where each electrode has a spatially uniform potential, the sum in Eq. (4) reduces to $C_x (R_\phi / d) \Delta_\phi$, where Δ_ϕ is the rotational dc imbalance in the four $x\phi$ electrodes (see Fig. 4) and we assume an infinite plate model for the capacitance derivatives.

The torque in Eq. (4), and likewise the associated random charge disturbance, is proportional to a net rotational dc bias imbalance, which can be compensated by counterbiasing the $x\phi$ sensing electrodes with the actuation circuitry. Figure 4 shows measured $1f_m$ torques as a function of the compensation voltage V_C. The measured torque is nulled very close to $V_C = 39$ mV (thus, $\Delta_\phi \approx -160$ mV), with balancing of the residual Δ_ϕ possible within 1 mV. An additional long measurement made for $V_C = 39$ mV has shown millivolt level stability in the residual imbalance over a 50 h period.

TABLE I. Electrostatic stiffness measurement results.

Component	Γ_s (fN m/mrad)	ϕ_0 (mrad)
$1f_m$	-89.76 ± 0.11	3.95 ± 0.01
$3f_m$	-89.3 ± 0.7	3.97 ± 0.07
$5f_m$	-92 ± 6	3.8 ± 0.4

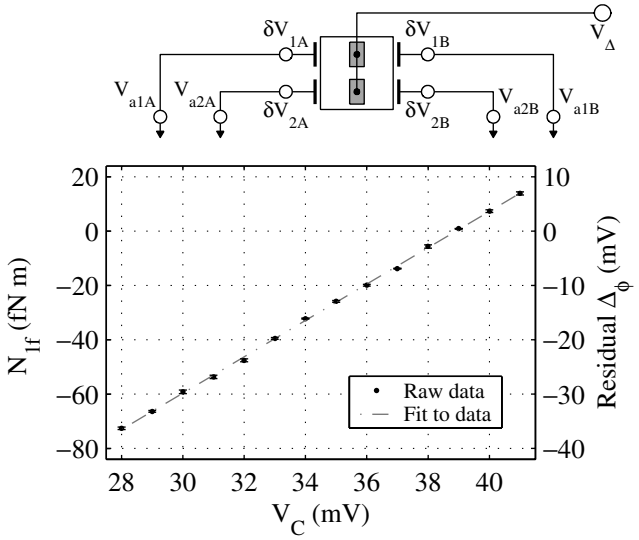

FIG. 4. Plot of dc bias measurement torques for applied bias amplitude $V_\Delta = 3V$ at $f_m = 5$ mHz, as a function of the applied dc compensation voltage V_C. The cartoon illustrates the measurement scheme, the average stray dc biases (with net rotational imbalance $\Delta_\phi \equiv \delta V_{1A} + \delta V_{2B} - \delta V_{1B} - \delta V_{2A}$), and the applied compensation voltages (here, we set $V_{a1A} = V_{a2B} = -V_{a1B} = -V_{a2A} = V_C$). The measured torque amplitude is proportional to a residual dc imbalance, which, for spatially uniform stray dc biases, is $\Delta_\phi + 4V_C$.

The results presented here, derived from measurements of torque on a suspended hollow test mass that is free only along a single rotational axis, merit some discussion concerning their representativity of the translational forces acting on an orbiting, solid Au/Pt LISA test mass. For the rotational stiffness measurement, Γ_s is proportional to the translational sensing stiffness k_s, with $\partial^2 C/\partial\phi^2$ replaced by $\partial^2 C/\partial x^2$ in Eq. (3). The sensor ac bias is likely the most dominant of several stiffness sources [10], and an apparatus upgrade permitting modulation of the sensor roation ϕ will allow measurement of the *total* stiffness. The measurements here confirm the sensor electrostatic model and convert to a translational stiffness uncertainty of 15 nN/m, roughly 5% of the total LISA stiffness budget [4].

The rotational dc bias measurement and compensation shown here is also directly applicable to the translational dc bias imbalance of relevance to LISA acceleration noise. Modulating V_Δ also excites a coherent force, detectable in flight [14], proportional to the translational imbalance Δ_x. The uniform potential model for Δ_ϕ is valid only as a rough number, as it neglects spatial surface potential variation. However, the measurement itself is sensitive to a sum over *all* surface domains, and thus the compensation V_C that nulls the modulated torque (or force) will also null the torque (or force) produced by test mass charging. Compensating a 100 mV level imbalance to within 1 mV reduces the potentially important random charging effect to an insignificant acceleration noise level.

The torque noise data can be cautiously converted into upper limits on specific contributions to the force noise f_n acting on LISA test masses. The hollow test mass used here is largely immune to gravitational or magnetic fields coupling to the bulk LISA test masses, and the torsional mode is insensitive to net forces from important linear temperature or field gradient effects [2]. This pendulum is designed for maximum sensitivity to surface forces, arguably the most dangerous and unpredictable sources for sensors with several millimeter gaps. Any electrostatic interaction between 100 kHz circuit noise and the sensor excitation, or between dc biases and low-frequency voltage noise, produces torque noise proportional to the net force noise. For these sources, the appropriate arm length for converting to force noise is the electrode half separation $R_\phi = 10.25$ mm, which gives a force noise upper limit of 1 pN/$\sqrt{\text{Hz}}$ between 0.6 and 10 mHz for such sources. Molecular impacts give force and torque noise on all test mass faces and have a 20 mm effective arm length, yielding a 500 fN/$\sqrt{\text{Hz}}$ upper limit from 0.6–10 mHz, with 250 fN/$\sqrt{\text{Hz}}$ around 3 mHz. This last number corresponds, for a solid Au/Pt test mass of the same dimensions, to acceleration noise of 200 fm/s^2/$\sqrt{\text{Hz}}$, a factor of 7 above the LTP flight goal.

We thank E. Adelberger and B. Hamilton for reviewing this manuscript and D. Shaul for electrostatic analysis. This work was supported by ESA, INFN, and ASI.

[1] P. Bender *et al.*, LISA ESA-SCI(2000)11, 2000.
[2] R. Dolesi *et al.*, Classical Quantum Gravity **20**, S99 (2003).
[3] B. Schumaker, Classical Quantum Gravity **20**, S239 (2003).
[4] D. Bortoluzzi *et al.*, Classical Quantum Gravity **20**, S89 (2003).
[5] J. Hanson *et al.*, Classical Quantum Gravity **20**, S109 (2003).
[6] G. L. Smith *et al.*, Phys. Rev. D **61**, 022001 (1999).
[7] M. Hueller *et al.*, Classical Quantum Gravity **19**, 1757 (2002).
[8] A. Cavalleri *et al.*, Classical Quantum Gravity **18**, 4133 (2001).
[9] W. J. Weber *et al.*, Classical Quantum Gravity **19**, 1751 (2002).
[10] W. J. Weber *et al.*, Proc. SPIE Int. Soc. Opt. Eng. **4856**, 31 (2002).
[11] D. N. A. Shaul and T. J. Sumner, Proc. SPIE Int. Soc. Opt. Eng. **4856**, 43 (2002).
[12] H. M. Araùjo, A. Howard, D. N. A. Shaul, and T. J. Sumner, Classical Quantum Gravity **20**, S311 (2003).
[13] P. L. Bender, Classical Quantum Gravity **20**, S305 (2003).
[14] W. J. Weber *et al.*, gr-qc/0309067 (to be published).